The Hybrid MHD-Gyrokinetic Code HMGC

G. Vlad[*]

[*]Associazione Euratom-ENEA sulla Fusione,
C.R. Frascati, Rome, Italy

in collaboration with S. Briguglio[*], G. Fogaccia[*], F. Zonca[*]
and B. Di Martino[†]

[†]Second University of Naples, Naples, Italy

III Convegno Nazionale su "La Fisica del Plasma in Italia"
L'Aquila, 20-22 Maggio 2002

Electronic version: http://fusfis.frascati.enea.it/~vlad/Miscellanea/slides_L'Aquila_2002.pdf

1 Outline

- Introduction
- The model
- Numerics
  - Fluid section
  - Gyrokinetic section: particle simulations, Particle-in-cell (PIC) vs. Finite-size-particle (FSP)
  - Parallelization: Domain vs. Particle decomposition
  - Parallel architectures: Distributed Memory, Shared Memory, Hierarchical Distributed-Shared Memory
- Examples

2 Introduction

- The Hybrid MHD-Gyrokinetic Code (HMGC) has been developped at the C.R. Frascati, ENEA laboratory in the frame of thermonuclear fusion research
- Recent experimental devices are approaching the so called ignition condition: fusion α-particles are confined in the toroidal (Tokamak) plasma and sustain the burning plasma
- Confinement properties of the energetic (α) particles are crucial in obtaining good performances in reactor relevant regimes
- Fusion α-particles are born mainly in the plasma centre, and the corresponding radial profile is peaked: their pressure gradient is a free-energy source that can destabilize waves which resonantly interact with the periodic motion of the energetic particles
- Energetic (hot) ions (α-particles) in plasmas close to ignition conditions have $v_H \approx v_A = B/\sqrt{4\pi n_i m_i}$.
- Interaction between energetic particles and shear Alfvén waves is likely to occur
- Shear Alfvén waves $\Longrightarrow$ Magnetohydrodynamic (MHD) model
- Energetic particles (wave-particle interaction) $\Longrightarrow$ Kinetic model
- Confinement properties of energetic particles $\Longrightarrow$ Nonlinear model

3 The model

- Bulk plasma: described by Magnetohydrodynamic (MHD) equations

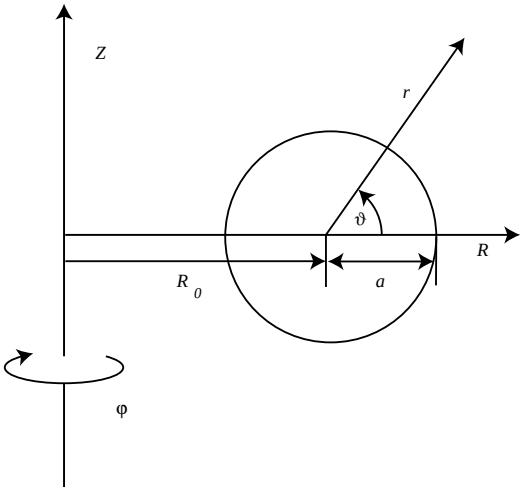

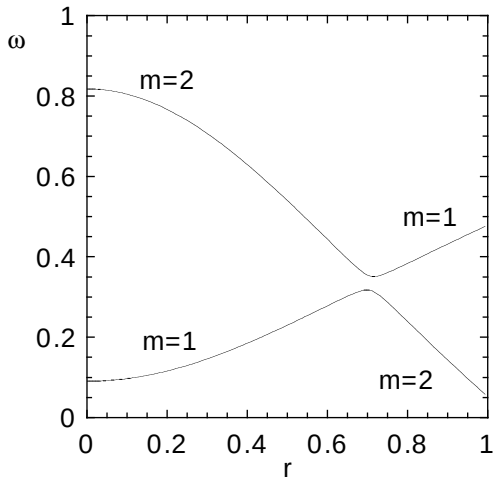

- Shear Alfvén waves in non-uniform equilibria exhibit a continuous spectrum: "local" plasma oscillations with frequency continuously changing throughout the plasma
- In toroidal geometry, the poloidal-symmetry breaking due to the toroidal field variation on a given magnetic flux surface cause different poloidal harmonics to be coupled: frequency "gap" appears in the Alfvén continuum
- Discrete, global MHD modes (Toroidal Alfvén Eigenmodes, or TAE's) can exist in the gaps of the shear-Alfvén frequency spectrum. TAE's are marginally stable MHD modes and can be easily driven unstable by the resonance with energetic particles
- Use reduced MHD equations expanded up to $O(\epsilon^3)$, with $\epsilon \equiv a/R_0$, a and R_0 the minor radius and the major radius of the torus, respectively, to keep toroidal effects in the model

- Hybrid MHD-kinetic models
  - Energetic particle density is typically much smaller than the bulk plasma density
  - Ordering:
$$\frac{n_H}{n_i} \approx O(\epsilon^3)\,, \quad \frac{T_H}{T_i} \approx O(\epsilon^{-2})$$
  - Thus, the following ordering for the ratio of the energetic to bulk ion β ($\beta \equiv 8\pi P_0/B_0^2$ is the ratio between the plasma kinetic and the magnetic pressures) follows:
$$\frac{\beta_H}{\beta_i} \approx O(\epsilon)$$
  - It can be shown that, making use of the above ordering, the MHD momentum equation is modified by a term which represent the perpendicular component of the divergence of the energetic-particle stress tensor $\mathbf{\Pi}_H$
  - Energetic-particle stress tensor obtained by solving Vlasov equation

- Particle simulation: gyrokinetic model

Direct solution of the equation describing the time evolution of the particle distribution function $F(t, Z)$ for collisionless plasmas:

Vlasov equation:

$$\frac{\partial F}{\partial t} + \frac{dZ^i}{dt}\frac{\partial F}{\partial Z^i} = 0\,,$$

Equations of motion:

$$\frac{dZ^i}{dt} = \dots\,.$$

Discretized form of $F(t, Z)$:

$$F(t,Z) \equiv \int dZ' F(t,Z')\delta(Z-Z') \approx \sum_{l=1}^{N} \Delta_l F(t,Z_l)\delta(Z-Z_l)\,.$$

Phase-space grid points $Z_l(t)$ evolve according to eqs. of motion: numerical particles. Gyrocenter coordinates $Z \equiv (\mathbf{R}, \mu, v_\parallel, \theta)$: $\mathbf{R}$ is the gyrocenter position, $v_\parallel$ parallel (to B) velocity, μ magnetic moment (exactly conserved in this coordinate system), θ the gyrophase (does not appear explicitly).

Volume elements $\Delta_l(t)$ evolve according to:

$$\frac{d\Delta_l}{dt} = \Delta_l(t)\left(\frac{\partial}{\partial Z^i}\frac{dZ^i}{dt}\right)_{t,Z_l(t)}\,.$$

Often it could be convenient to evolve only the perturbed part δF of the distribution function:

$$\Longrightarrow \qquad F(t,Z) = F_0(t,Z_l) + \delta F(t,Z_l)$$

4 Particle-in-cell versus Finite-size-particle

Plasma condition $n_0\lambda_D^3 \gg 1$ (collective interaction dominate over collisions) implies a huge number of simulation particles. Even assuming $n_s\lambda_D^3 \approx 10$, typically ($L_{eq}$ equilibrium length):

$$N_{part} \approx n_s L_{eq}^3 = n_s\lambda_D^3 \left(L_{eq}/\lambda_D\right)^3 \approx 10^{13}\,.$$

Violation of plasma condition $n_0\lambda_D^3 \ll 1$: system too collisional, short range interactions between particles dominate over the long range ones.

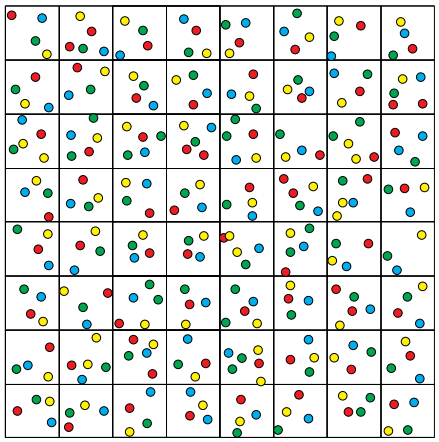

Particle-in-cell (PIC)

1. Electromagnetic fields computed at the points of a discrete spatial grid
2. Interpolation of the e.m. fields at the (continuous) particle positions to compute the forces and perform particle pushing
3. Pressure contribution of energetic particle calculated at the grid points to close the equations

$\Longrightarrow$ Short-range interactions are then cut off for mutual distances shorter than the typical spacing – L_c – between grid points, whilst the relevant long-range interactions are not significantly affected.
$\Longrightarrow$ PIC particle ensemble behaves as a plasma under the much more relaxed condition $n_0 L_c^3 \gg 1$ (with $L_c \gg \lambda_D$)

- Finite-size-particle (FSP)

Finite-size-particles (charge clouds):

$$n_s(x) = \sum_l \Delta_l \delta(x - x_l) \qquad \longrightarrow \qquad \sum_l \Delta_l S(x - x_l)$$

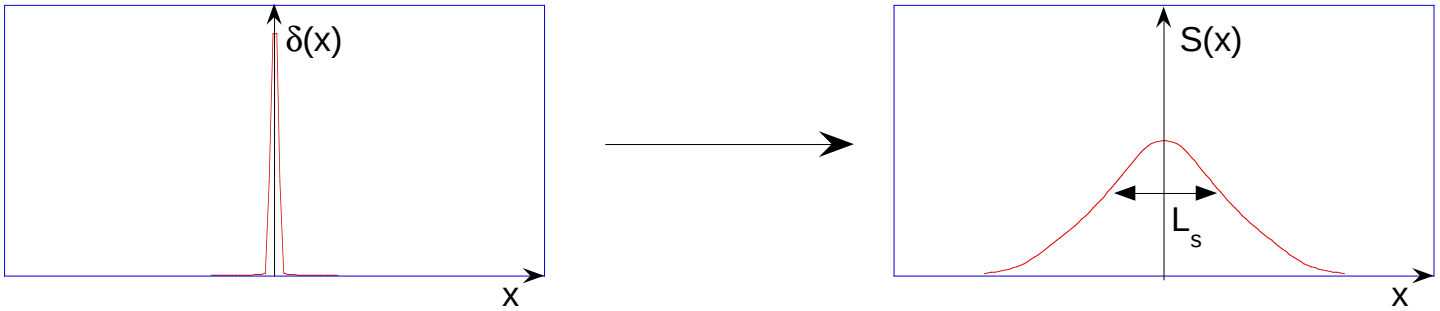

The spatial characteristic width of the cloud $\lambda_D \ll L_s \ll L_{eq}$ restricts the maximum spatial resolution attainable in the simulation (assuming $L_{eq}/L_s \approx 100$, $n_s\lambda_D^3 \approx 10$):

$$n_s\lambda_D^3 \gg 1 \longrightarrow n_s L_s^3 \gg 1\,, \quad N_{part} \approx n_s L_s^3 \left(L_{eq}/L_s\right)^3 \approx 10^7\,.$$

L_s plays the role of L_c

5 Computational loads and Parallelization

Assume that field solver uses Fourier transform to solve the MHD equations.
Serial code, number of operations (O) per time step and memory (M) required:
PIC:

$$O^{PIC} \approx f\left(N_{harm}\right) + n_{FT} \times N_{harm} \times N_{cell} + n_{int} \times N_{part}\,,$$
$$M^{PIC} \approx m_{harm} \times N_{harm} + m_{cell} \times N_{cell} + m_{part} \times N_{part}\,,$$

N_{harm}: number of Fourier harmonics retained in the simulation; $f\left(N_{harm}\right)$: operations for the solution of the field solver; n_{FT}: number of operations needed to compute each addendum in the Fourier transform; N_{cell}: number of cells of the spatial grid; n_{int}: operations for the field interpolation; N_{part}: number of simulation particles; m_{harm}, m_{cell} and m_{part}: memory needed to store, respectively, a single harmonic of the complete set of Fourier-space fields, the real-space fields at each grid point and the phase-space coordinates for each particle.
FSP:

$$O^{FSP} \approx f\left(N_{harm}\right) + n_{FT} \times N_{harm} \times N_{part}\,,$$
$$M^{FSP} \approx m_{harm} \times N_{harm} + m_{part} \times N_{part}.$$

Typically, $f\left(N_{harm}\right)$ negligible in comparison with terms $\propto N_{part}$; for PIC codes, $N_{ppc} \equiv N_{part}/N_{cell} \approx n_0 L_c^3 \gg 1$: as far as $n_{FT} \times N_{harm} \gg n_{int}$ the gridless FSP method is more expensive than the PIC one, without presenting any significant advantage in terms of memory requests.

Two distinct reasons could however justify a different trend:

1. Interest in simplified simulations in which only very few modes are evolved: linear simulations, or weak nonlinear coupling (nonlinear mode spectrum restricted to a limited number of significant harmonics): in such a few-harmonic framework, the condition $n_{FT} \times N_{harm} \gg n_{int}$ can be violated or, at least, significantly weakened;

2. schemes of parallelization (distributed-memory architectures):
   domain decomposition ($d.d.$) versus particle decomposition ($p.d.$)

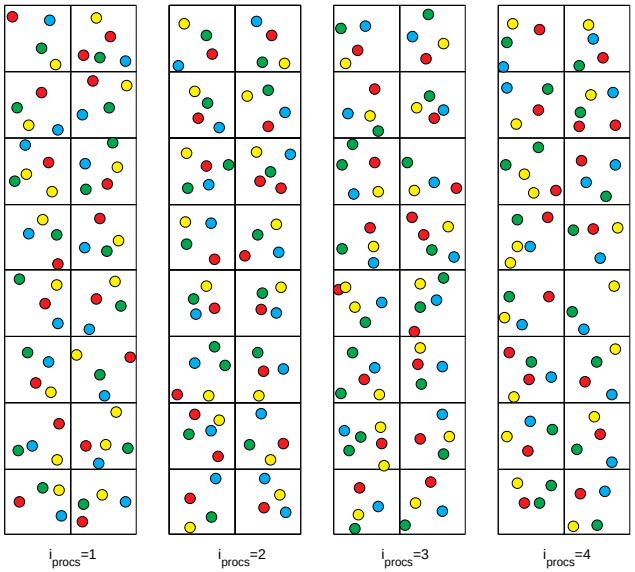

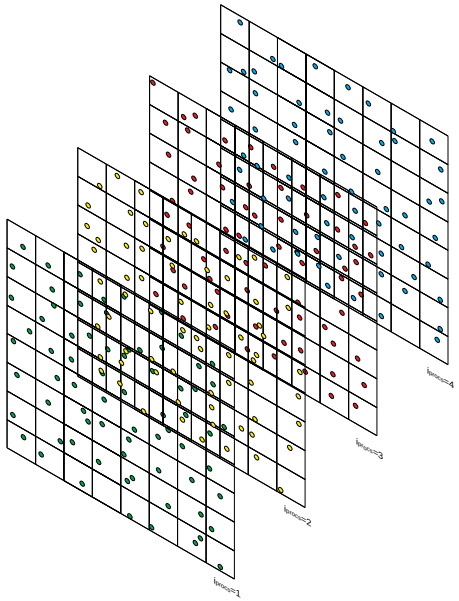

Domain decomposition, PIC

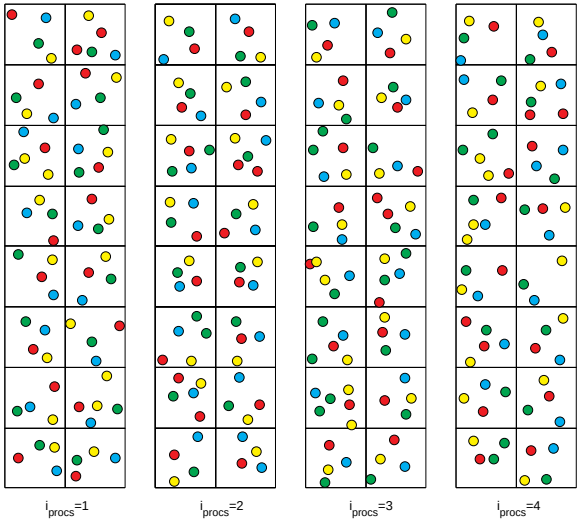

Different portions of the physical domain are assigned to different processors, together with the particles that reside on them.

$$O_{d.d.}^{PIC} \approx f\left(N_{harm}\right) + \frac{1}{n_{proc}}\left(n_{FT} \times N_{harm} \times N_{cell} + n_{int} \times N_{part}\right) ,$$

$$M_{d.d.}^{PIC} \approx m_{harm} \times N_{harm} + \frac{1}{n_{proc}}\left(m_{cell} \times N_{cell} + m_{part} \times N_{part}\right) .$$

Advantages: almost linear scaling of the attainable physical-space resolution (more precisely, the maximum number of spatial cells) with the number of processors.

Disadvantages: particle migration from one portion of the grid to another, possible severe load-balancing problems $\Longrightarrow$ dynamical redistribution of grid and particle quantities is required, which makes the parallel implementation of a PIC code very complicate.

Particle decomposition, PIC

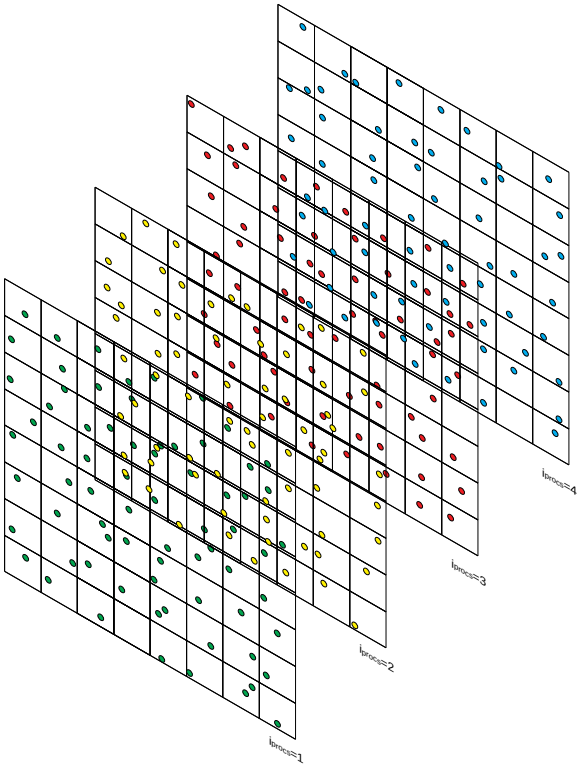

Statically distributing the particle population among processors, while replicating the data relative to grid quantities. Before updating the electromagnetic fields, at each time step, partial contributions to particle pressure coming from different portions of the population must be summed together (reduction).

$$O_{p.d.}^{PIC} \approx f\left(N_{harm}\right) + n_{FT} \times N_{harm} \times N_{cell} + n_{int} \times \frac{N_{part}}{n_{proc}},$$

$$M_{p.d.}^{PIC} \approx m_{harm} \times N_{harm} + m_{cell} \times N_{cell} + m_{part} \times \frac{N_{part}}{n_{proc}}.$$

Advantages: load balancing is automatically enforced; parallelization is, in principle, almost straightforward. It is very efficient if computational load related to particles dominates, for each processor, the one related to the grid ($n_{proc} \lesssim N_{ppc}$).

Disadvantages: grid calculations do not take advantage, with regard both to the number of operations and the memory requests, from such a parallelization: each processor has to handle the whole spatial domain. Even neglecting efficiency problems, high spatial-resolution levels are limited by the single node RAM.

Particle decomposition, FPS

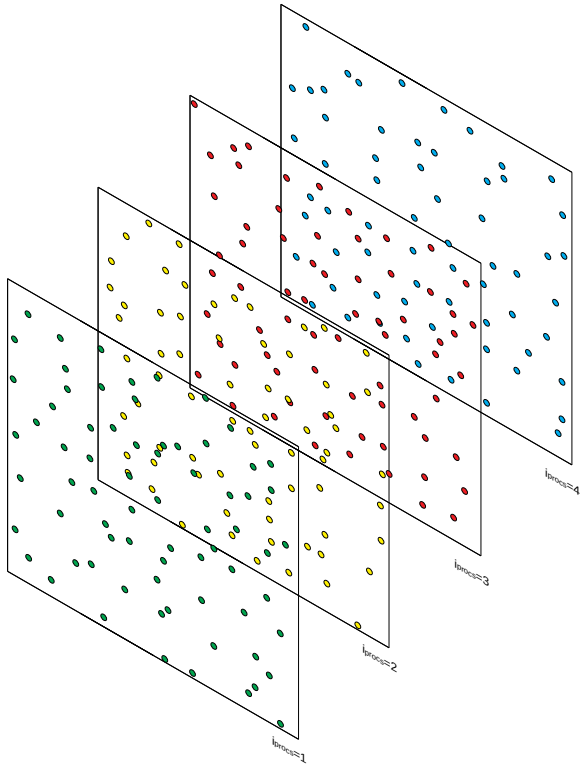

bottle-necks in efficiency and performance associated to grid quantities induces one to by-pass the introduction of a spatial grid, so resorting to the gridless FSP simulation:

$$O_{p.d.}^{FSP} \approx f\left(N_{harm}\right) + n_{FT} \times N_{harm} \times \frac{N_{part}}{n_{proc}}\,,$$

$$M_{p.d.}^{FSP} \approx m_{harm} \times N_{harm} + m_{part} \times \frac{N_{part}}{n_{proc}}\,.$$

Advantages: Fourier transforms are distributed among the processors. High spatial resolution can be obtained. Massively parallel simulations can yield significant benefits as far as the number of modes, N_{harm}, retained in the simulation is relatively small, in spite of the high mode numbers considered (high spatial resolution).
Disadvantages: few-harmonic limitation.

6 HMGC Parallel architectures

- The HMGC code exists in a PIC version and in a gridless FSP version.
- Parallel implementations include:
  - Distributed Memory (IBM SP, cluster of workstations),
  - Shared Memory (Symmetric Multiprocessor Systems, SMPs),
  - Hierarchical distributed-shared memory multiprocessor architectures (IBM SP, cluster of SMPs).

Level	INTER-NODE
Language	HPF
Strategy	Particle Decomposition

Level	INTRA-NODE			
Language	OpenMP			
Phase	Particle pushing	Pressure updating	*Variant*	*Version*
Strategy	Particle decomposition	Particle decomposition	Critical	–
			Auxiliary array `p_aux`	*v1*
		Domain decomposition	Sorting	*v2a*
			Selective sorting	*v2b*

7 Results

Fluid nonlinearities: saturation of a TAE ($\omega = \omega_0 \approx 0.33\,\omega_A$)

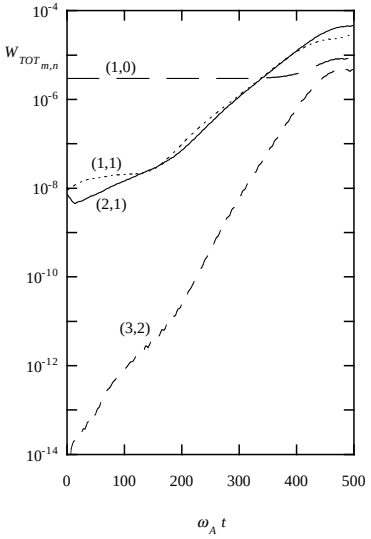

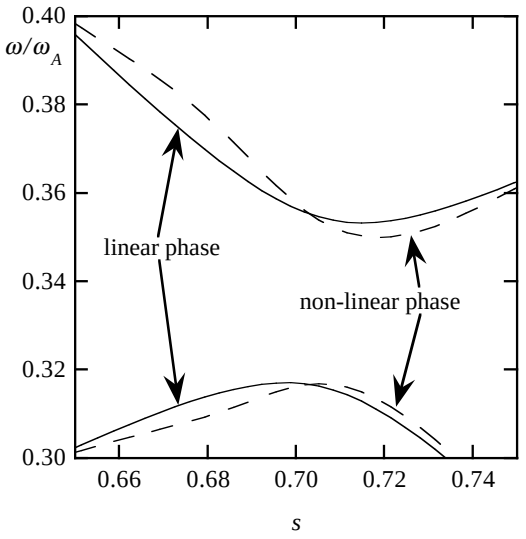

Volume integrated energy (magnetic plus kinetic) for different Fourier components (m, n) vs. time for a non-linear simulation of an unstable driven TAE. The q-profile has a parabolic radial dependence with $q(0) = 1.1$ and $q(a) = 1.9$. The inverse aspect ratio is $\epsilon = 0.075$, the density is constant $\hat{\varrho} = \hat{\varrho}_0$ and the resistivity corresponds to $S^{-1} = 10^{-5}$.
Blow-up of the Alfvén continuum. The continuous spectra obtained in the linear limit and at the beginning of the non-linear phase are compared.

Kinetic nonlinearities: gap-mode saturation ($\omega = \omega_0 \approx 0.33\,\omega_A$)

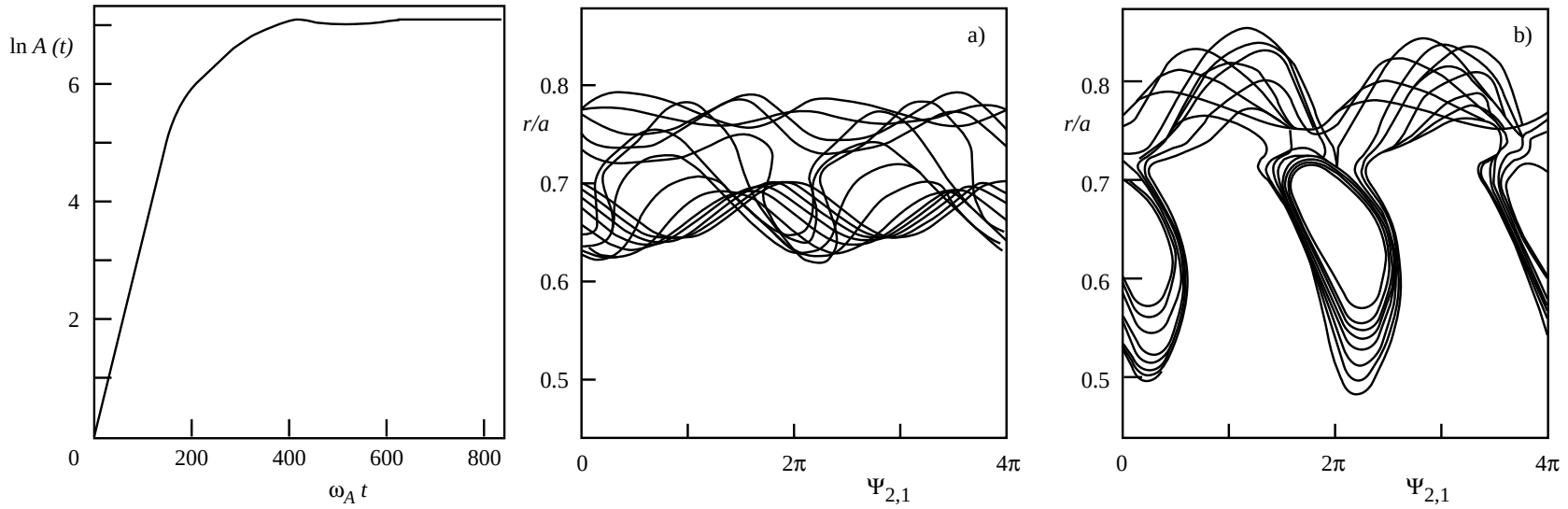

Time evolution of the mode amplitude $A(t)$ for a perturbative non-linear simulation with $\gamma_D = 0.01\,\omega_A$, $\beta_H(0) = 0.08$.
Orbit in the plane $(\Psi_{2,1}, r)$ ($\Psi_{m,n} \equiv \omega_r t - m\vartheta + n\varphi$), for a test particle, in the time intervals $0 < \omega_A t < 284$ (a) (linear growth) and $264 < \omega_A t < 560$ (b) (non-linear saturation). The $\Psi_{2,1}$ axis is mapped onto the interval $0 \leq \Psi_{2,1} < 4\pi$. The particle is initially passing, but becomes trapped as the mode reaches a certain amplitude.

Transition from Kinetic TAE to EPM (Energetic Particle Mode):

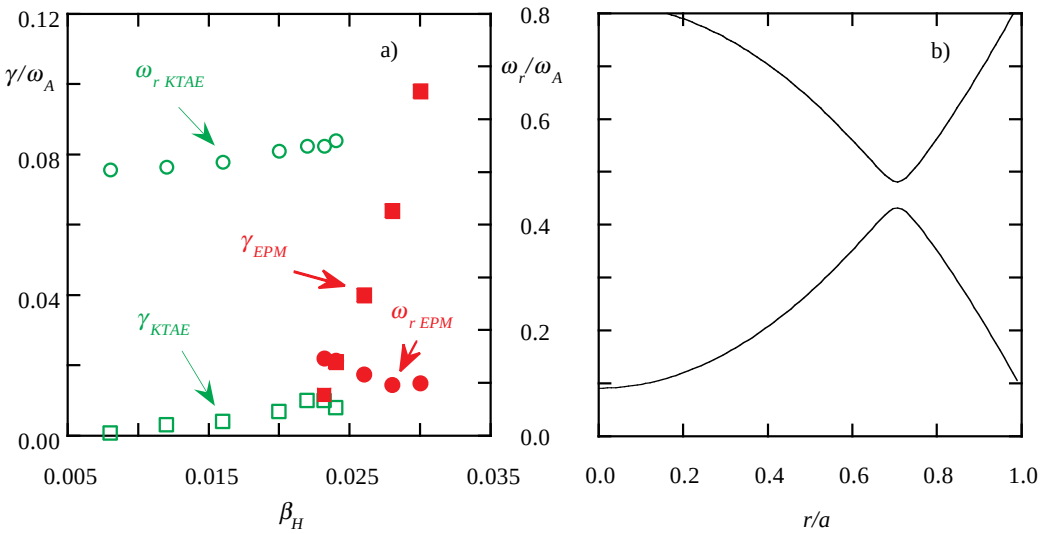

β-threshold vs. toroidal mode number n:

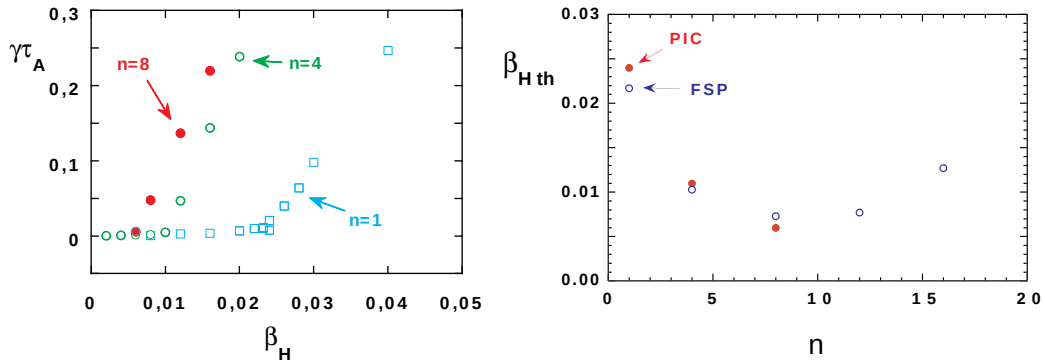

Nonlinear EPM saturation generating shear flows ($n = 8$, monotonic $q(r)$ profile, $q(0) = 1.1$, $q(a) = 1.9$, $N_{part} \approx 16.7 \times 10^6$): see movie:
http://fusfis.frascati.enea.it/~vlad/Miscellanea/EPM_MOVIES/n8_9_imirr1_13_zonal_3x4.mov

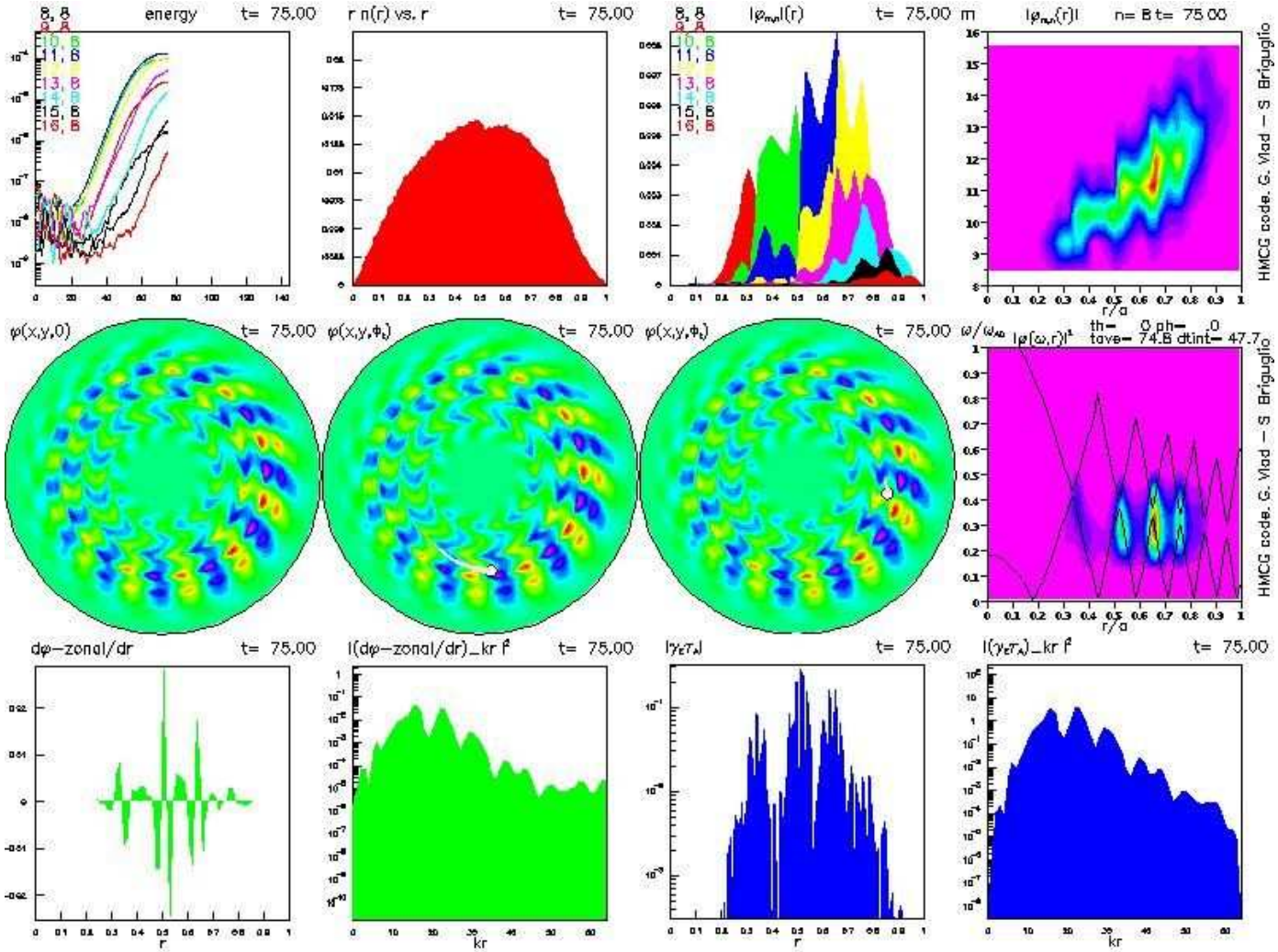

Deeply hollow q profile

- Deeply hollow q profile ($q(0) \approx 5$, $q_{min} = 2.1$, $q(a) \approx 5$, profile (a)), $\beta_H(0) = 2.5\%$.
- $\omega_{gap}/\omega_{A,r=0} = 1/(2q(r)\sqrt{\rho/\rho_{r=0}})$: assume first a radially constant thermal-plasma density ρ $\Rightarrow$ radially constant Alfvén velocity (such an assumption will be removed later).

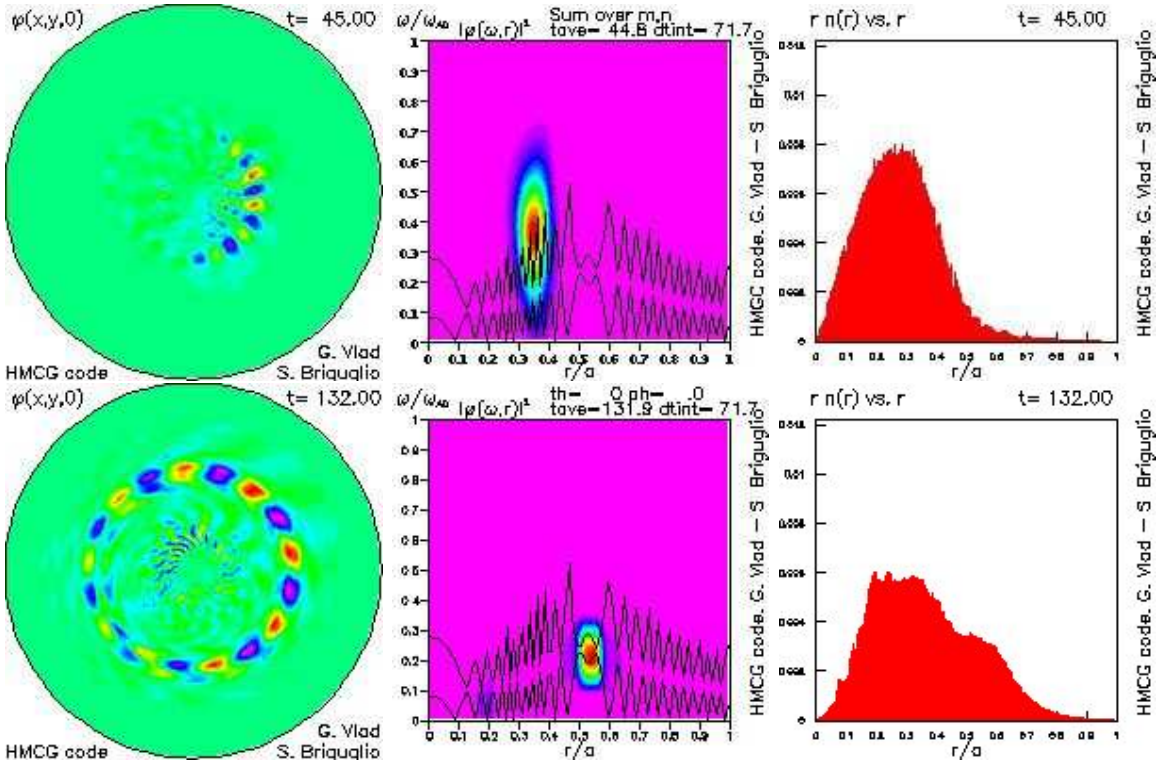

see movie:
http://fusfis.frascati.enea.it/~vlad/Miscellanea/IAEA-Goteborg/n4_JET_7.mov

- After a transient initial phase, a mode localized around the maximum β'_H emerges at $r \approx 0.35a$, with frequency well inside the continuum. We can identify this mode as an Energetic Particle continuum Mode (EPM).
- Its saturation takes places because of a strong (convective) outward radial displacement of the energetic ions.
- As such a displacement takes place, the local drive is reduced due to the flattening of the energetic-ion density profile. The drive is no longer able to overcome the strong continuum damping at the original frequency.
- The maximum of the power spectrum migrates towards the gap (in order to minimize the continuum damping), but it also moves outwards, following the displaced source, in order to maximize the drive.
- The mode reaches the gap and it localizes around the zero-shear, q_{min} surface ($r \approx 0.5a$).

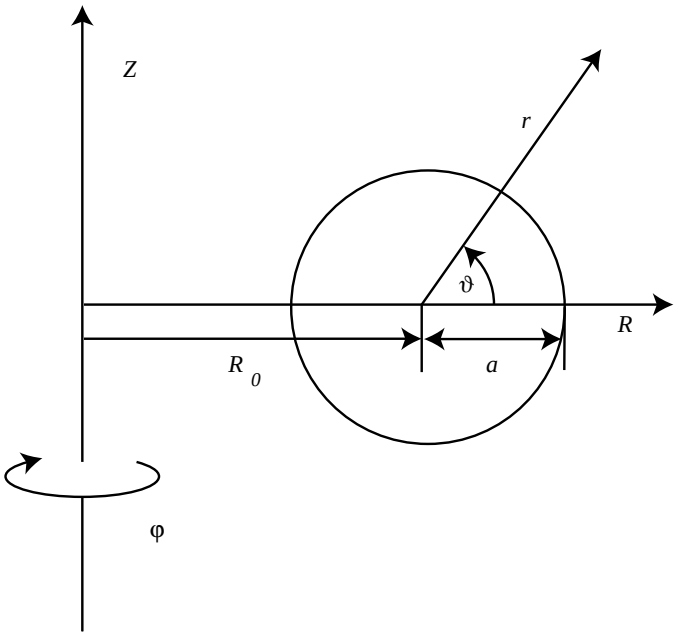

Low-β tokamak ordering ($\beta \equiv 8\pi P_0/B_0^2$ is the ratio between the plasma kinetic and the magnetic pressures):

$$\frac{v_\perp}{v_A} \approx \frac{B_\perp}{B_\varphi} \approx \frac{\mathbf{B}/B \cdot \nabla}{\nabla_\perp} \approx O(\epsilon)\,,$$

$$\frac{v_\varphi}{v_A} \approx \frac{\nabla \cdot \mathbf{v}_\perp}{v_A/a} \approx \frac{\nabla(RB_\varphi)}{B_\varphi} \approx O(\epsilon^2)\,, \qquad \frac{\partial}{\partial t} \approx \frac{v_A}{R}\,.$$

Here, a cylindrical-coordinate system (R, Z, φ) has been used, and the subscript $\perp$ denotes components perpendicular to $\nabla\varphi$. The magnetic field can be written as

$$\mathbf{B} = \left(F_0 + \tilde{F}\right)\nabla\varphi + R_0\nabla\psi \times \nabla\varphi + O(\epsilon^3 B_\varphi)$$

where ψ is the poloidal magnetic flux function, $F_0 = R_0 B_0$, B_0 is the vacuum (toroidal) magnetic field at $R = R_0$, and $\tilde{F} \approx O(\epsilon^2 F_0)$ is given, at the leading order, by equilibrium corrections.

- Reduced MHD equations:

$$\frac{\partial \psi}{\partial t} = -\frac{cR^2}{R_0 B_0}\nabla\psi \times \nabla\varphi \cdot \nabla\phi - \frac{c}{R_0}\frac{\partial \phi}{\partial \varphi} + \eta\frac{c^2}{4\pi}\Delta^*\psi + O(\epsilon^4 v_A B_\varphi)\,,$$

$$\hat{\varrho}\left(\frac{D}{Dt} - \frac{2c}{R_0 B_0}\frac{\partial \phi}{\partial Z}\right)\nabla_\perp^2\phi + \nabla\hat{\varrho}\cdot\left(\frac{D}{Dt} - \frac{c}{R_0 B_0}\frac{\partial \phi}{\partial Z}\right)\nabla\phi =$$
$$-\frac{B_0}{4\pi c}\mathbf{B}\cdot\nabla\Delta^*\psi - \frac{B_0}{cR_0}\nabla\cdot\left[R^2\left(\nabla P + \nabla\cdot\mathbf{\Pi}_H\right)\times\nabla\varphi\right] + O(\epsilon^4\varrho\frac{v_A^2 B_\varphi}{a^2 c})\,,$$

$$\frac{DP}{Dt} = O(\epsilon^4\frac{v_A B_\varphi^2}{a})\,,$$

with η the plasma resistivity,

$$\mathbf{v}_\perp = -\frac{cR^2}{R_0 B_0}\nabla\phi\times\nabla\varphi + O(\epsilon^3 v_A)\,,\quad \hat{\varrho} = \frac{R^2}{R_0^2}\varrho\,,\qquad \frac{D}{Dt} = \frac{\partial}{\partial t} + \mathbf{v}_\perp\cdot\nabla\,,$$

$$\nabla_\perp^2 \equiv \frac{1}{R}\frac{\partial}{\partial R}R\frac{\partial}{\partial R} + \frac{\partial^2}{\partial Z^2}\,,\quad \Delta^*\psi = R^2\nabla\cdot\left(\frac{\nabla\psi}{R^2}\right) = R\frac{\partial}{\partial R}\left(\frac{1}{R}\frac{\partial\psi}{\partial R}\right) + \frac{\partial^2\psi}{\partial Z^2}\,.$$

- Particle simulation target: obtaining from the numerical plasma the same behaviour of the physical one

It is impossible to simulate, with today numerical resources, the number of particles of real plasmas

Consider the Debye length λ_D and the Larmor radius ρ_L:

$$\lambda_D = \left(\frac{T}{4\pi e^2 n}\right)^2 , \quad \rho_L = \frac{c(mT)^2}{eB}$$

Consider mutually interacting macroparticles:

$$n_s = \frac{n_f}{M} , \quad M \gg 1 , \quad e_s = M e_f , \quad m_s = M m_f , \quad v_s = v_f$$
$$\Longrightarrow T_s \propto m_s v_s^2 = M m_f v_f^2 \propto M T_f \quad \Longrightarrow \lambda_{D,s} = \lambda_{D,f} , \quad \rho_{L,s} = \rho_{L,f}$$

Plasma condition $n_0 \lambda_D^3 \gg 1$ (collective interaction dominate over collisions) implies a huge number of simulation particles. Even assuming $n_s \lambda_D^3 \approx 10$, typically ($L_{eq}$ equilibrium length):

$$N_{part} \approx n_s L_{eq}^3 = n_s \lambda_D^3 \left(L_{eq}/\lambda_D\right)^3 \approx 10^{13} .$$

Violation of plasma condition $n_0 \lambda_D^3 \ll 1$: system too collisional, short range interactions between particles dominate over the long range ones.

The pressure tensor is:

$$\begin{aligned}\mathbf{\Pi}_H\left(t,\mathbf{x}\right) &= \frac{1}{m_H^2}\int d^6\overline{Z}D_{z_c\rightarrow\overline{Z}}\overline{F}_H\left(t,\overline{\mathbf{R}},\overline{M},\overline{U}\right)\times \\ &\quad \left[\frac{\Omega_H\overline{M}}{m_H}\mathbf{I}+\hat{\mathbf{b}}\hat{\mathbf{b}}\left(\overline{U}^2-\frac{\Omega_H\overline{M}}{m_H}\right)\right]\delta\left(\mathbf{x}-\overline{\mathbf{R}}\right),\end{aligned}$$

Equation of motion for energetic particles:

$$\begin{aligned}\frac{d\overline{\mathbf{R}}}{dt} &= \overline{U}\hat{\mathbf{b}}+\frac{e_H}{m_H\Omega_H}\hat{\mathbf{b}}\times\nabla\phi-\frac{\overline{U}}{m_H\Omega_H}\hat{\mathbf{b}}\times\nabla a_{\parallel}+ \\ &\quad \left[\frac{\overline{M}}{m_H}+\frac{\overline{U}}{\Omega_H}\left(\overline{U}+\frac{a_{\parallel}}{m_H}\right)\right]\hat{\mathbf{b}}\times\nabla\ln B, \\ \frac{d\overline{M}}{dt} &= 0, \\ \frac{d\overline{U}}{dt} &= \frac{1}{m_H}\hat{\mathbf{b}}\cdot\left\{\left[\frac{e_H}{\Omega_H}\left(\overline{U}+\frac{a_{\parallel}}{m_H}\right)\nabla\phi+\frac{\overline{M}}{m_H}\nabla a_{\parallel}\right]\right. \\ &\quad \times\ \left.\nabla\ln B+\frac{e_H}{m_H\Omega_H}\nabla a_{\parallel}\times\nabla\phi\right\}-\frac{\Omega_H\overline{M}}{m_H}\hat{\mathbf{b}}\cdot\nabla\ln B.\end{aligned}$$